ARCTIC
VOL. 47, NO. 3 (SEPTEMBER 1994) P. 280–287

On the Validation of Satellite-Derived Sea Ice Surface Temperature

J. KEY,[1] J.A. MASLANIK,[1] T. PAPAKYRIAKOU,[2] M.C. SERREZE[1] and A.J. SCHWEIGER[3]

(Received 5 May 1993; accepted in revised form 14 October 1993)

ABSTRACT. The surface temperature of sea ice controls the rate of ice growth and heat exchange between the ocean and the atmosphere. An algorithm for the satellite retrieval of ice surface temperature has recently been published, but due to the lack of validation data has not been extensively tested. In this paper, data from a recent Arctic field experiment is used in an attempt to validate that algorithm. While the procedure is, in principle, straightforward, we demonstrate that validation is complicated by a variety of factors, including incorrectly assumed atmospheric conditions, undetected clouds in the satellite data, spatial and temporal variability in the surface temperature field, and surface and satellite measurement errors. Comparisons between surface temperatures determined from upwelling broadband longwave radiation, spatial measurements of narrow-band radiation, thermocouples buried just below the snow surface, and narrow-band satellite data show differences of 1 to 3˚C. The range in these independent measurements indicates the need for specially designed validation experiments utilizing narrow-band radiometers on aircraft to obtain broad spatial coverage.

Key words: ice surface temperature, Arctic climate, sea ice, AVHRR

RÉSUMÉ. La température de la surface de la glace de mer contrôle le taux de croissance de la glace et les échanges thermiques entre l'océan et l'atmosphère. Un algorithme d'extraction par satellite de la température de la surface de la glace a récemment été publié, mais n'a pu être mis à l'essai sur une grande échelle, en raison du manque de données de validation. On tente, dans cet article, de valider cet algorithme à l'aide de données provenant d'une expérience de terrain menée récemment dans l'Arctique. Si la procédure est, en principe, simple, on démontre que divers facteurs viennent compliquer cette validation, dont une évaluation incorrecte des conditions atmosphériques, la présence de nuages non détectés dans les données obtenues par satellite, une variabilité spatiale et temporelle dans la température de surface de l'aire expérimentale, et des erreurs dans les mesures prises sur le terrain même et par satellite. Des comparaisons entre les températures de surface déterminées à partir du rayonnement ascendant des ondes longues à large bande, des mesures spatiales du rayonnement à bande étroite, des thermocouples placés juste sous la surface de la neige et des données de satellite dans la bande étroite révèlent des différences allant de 1 à 3 ˚C. La différence qui existe dans ces mesures prises indépendamment montre bien la nécessité de mettre sur pied des expériences de validation conçues à des fins spécifiques, qui utilisent des radiomètres à bande étroite sur les avions en vue d'obtenir une grande couverture spatiale.

Mots clés: température de la surface de la glace, climat de l'Arctique, glace de mer, radiomètre perfectionné à très haute résolution

Traduit pour la revue *Arctic* par Nésida Loyer.

INTRODUCTION

Ice surface temperature (IST) controls the rate of sea ice growth and air-sea heat exchange and is therefore an important parameter to monitor for climate change studies. Little effort has been directed to the retrieval of the sea ice surface temperature in the Arctic, an area where the effects of greenhouse warming may be most pronounced. Our limited knowledge of atmospheric temperature, humidity, and aerosol profiles, cloud microphysical properties, and the spectral characteristics of the wide variety of surface types found there has hindered the satellite retrieval of IST. Recently, however, Key and Haefliger (1992) used Arctic data to develop an IST retrieval algorithm using thermal data from the Advanced Very High Resolution Radiometer (AVHRR) on-board the U.S. National Oceanic and Atmospheric Administration's (NOAA) polar-orbiting satellites. Nevertheless, as few validation data were available for that study, biases in IST estimates due to sensor calibration, unmodeled atmospheric effects, and other factors could not be assessed. Such an assessment is crucial if IST is to be used as a climate change indicator.

Here we report on the application and validation of the IST retrieval procedure using a suite of *in situ* data collected during the May-June 1992 Seasonal Sea Ice Monitoring and Modeling Site (SIMMS) field campaign. Satellite-derived estimates of IST are compared to near-surface air temperatures, surface temperatures derived from upwelling longwave (broadband) radiation measurements, and from a thermocouple just below the snow surface. Since the satellite field of view (FOV) is at best 1.1 km, comparisons are also made with surface temperature estimates collected over an approximately 1 km^2 area with a hand-held infrared thermometer. The problems encountered are not unlike those experienced in the validation of sea surface temperatures, where there are a variety of ways of measuring the surface temperature *in situ* (Wick *et al.*, 1992). Throughout this paper the

[1] Cooperative Institute for Research in Environmental Sciences, University of Colorado, Campus Box 449, Boulder, Colorado 80309, U.S.A.
[2] Earth Observations Laboratory, University of Waterloo, Waterloo, Ontario N2L 3G1, Canada
[3] Polar Science Center, University of Washington, Seattle, Washington 98105, U.S.A.

"surface" temperature refers to the skin or radiating temperature of the snow or ice surface.

METHODS

In situ Measurements

Surface microclimate data were collected during the SIMMS'92 field experiment. The first-year ice (FYI) site [74°41.66′N, 95°35.22′W] was the focus of the measurement program and operated from 19 April to 26 June. Air temperatures were measured with thermocouple sensors. All sensors are accurate to within approximately 0.3°C. The sensors were housed within ventilated phychrometer shieldings. While air temperatures were measured at five vertical levels, the air temperature sensor used for this study (Ta1) ranged in height between 54 cm and 57 cm above the snow surface from 10 May to 24 May, and between 47 cm and 65.5 cm after 24 May to the end of the experiment. As with air temperatures, snow temperatures were measured in profile within the snow cover, extending from the snow/ice interface to near the snow surface, using a thermocouple epoxied in the tip of white plastic tubing (20 cm × 0.5 cm). All sensors and leads were painted white. The temperature from the thermocouple nearest the surface, the depth of which varied from 0 to 3 cm, is used here.

Downwelling sky and surface emitted broadband infrared radiation (4-50 μm) were measured with Eppley Precision Infrared Radiometers (model PIR). One of these pyrgeometers was mounted on an extension arm approximately 8.9 m from the snow surface on an instrument tower. A sky-facing pyrgeometer was mounted on a post, approximately 35 m west of the instrument tower. Instrument height was approximately 1.5 m above the snow surface. The manufacturer indicates the thermopile response to be within 1% linearity to calibration. The flux measurement was corrected for the infrared radiation emitted by the thermopile using the Stefan–Boltzman equation and a measure of the internal instrument temperature as recorded using the precision thermistor (YSI 44031) housed within the instrument. Thermistor tolerance is approximately 0.125°C between -10° and -20°C; however, the measurement error is probably closer to ±0.2°C when logged to the 21X micrologger. Regardless of these specifications, the accuracy of the instrument is difficult to quantify because of possible heating of the instrument dome due to absorbed incident shortwave radiation (Weiss, 1981, 1982; Berdahl and Fromberg, 1982; Ryznar and Weber, 1982); consequently, the temperature of the dome was also monitored in order to assess the degree to which any heating of the dome may bias the flux measurements.

All sensors at the FYI site microclimate station were logged to Campbell Scientific Instruments dataloggers. Instruments were scanned at five second intervals, and data were stored as 30 minute averages.

The surface thermodynamic temperature based on pyrgeometer data, T_{pyrg}, was estimated from the upwelling longwave radiation emitted by the surface, $L\uparrow_{surf}$ according to the Stefan-Boltzman law:

$$T_{pyrg} = \left(\frac{L\uparrow_{surf}}{\sigma\varepsilon} \right)^{\frac{1}{4}} - 273.15 \qquad [1]$$

where T_{pyrg}, is in degrees C, σ is Boltzman's constant, and ε is the emissivity, taken to be 0.99 here. However, because the emissivity is less than unity, the upwelling radiation measured by the sensor, $L\uparrow$, is the sum of the radiation emitted by the surface, $L\uparrow_{surf}$, and that portion of the downwelling atmospheric radiation, $L\downarrow$, that is reflected by the surface:

$$L\uparrow = L\uparrow_{surf} + (1-\varepsilon)L\downarrow \qquad [2]$$

so that this reflected component must be removed from the upwelling radiance before calculating the surface temperature. The discussion in the appendix suggests that the uncertainty surrounding our T_{pyrg} estimate is approximately ±0.2°C.

In order to characterize the spatial variability of the temperature field over an area comparable to an AVHRR pixel, skin temperatures measured with an infrared (IR) thermometer ($T_{IRtherm}$) and snow/ice interface temperatures ($T_{s\text{-}i}$) were measured along transects within the 1 × 1 km sample site and the multi-year site. Each set of surface observations at the FYI site consisted of measurements spaced 200 m apart along two randomly selected 1 km transects, with the time between measurements kept to a minimum. The typical time required to cover the ten stops was about 90 minutes, with sampling times selected to correspond to AVHRR overpasses whenever possible. $T_{IRtherm}$ was measured with an Everest™ hand-held IR thermometer; a non-contact instrument that determines a brightness temperature of the object within the instrument's field of view based on received radiation in the 8 – 14 μm range. The instrument is factory-calibrated to yield a representative accuracy of 0.5kC in an operating environment of 0° to 50°C. The manufacturer estimates that accuracy below 0°C is approximately the same. The instrument was tested periodically by measuring the temperature of fresh water at its freezing point in a slush bucket, where the IR thermometer typically yielded temperatures of ±0.3°C. During measurements along the transects, the IR thermometer was allowed to reach equilibrium temperature with its surroundings. Measurements were taken with the IR thermometer held about 1 m from the surface at an angle to the surface of approximately 45°. Emissivity of the snow-covered sea ice was set at 0.99.

AVHRR-derived Ice Surface Temperatures

The general approach to estimating surface temperature is to relate satellite observations to surface temperature observations with a regression model (e.g., Barton, 1992). Lacking sufficient observations, however, satellite radiances or brightness temperatures can be modeled by application of the radiative transfer equation. This "forward model" approach is commonly used for retrieval of sea surface temperature and forms the basis for the Key and Haefliger (1992) IST algorithm. The procedure corrects for the atmospheric attenuation of satellite-measured clear sky brightness temperatures in the AVHRR split-window thermal channels (channels 4 and 5 at approximately 11 μm and

12 μm). These corrections are specified for three different "seasons" and as a function of satellite viewing angle, and are expected to be applicable to the perennial ice pack in the central Arctic Basin. This is not a completely new methodology; instead, it is a modification of a standard procedure for use with Arctic-specific data.

For the retrieval of IST we use the methodology of Key and Haefliger (1992), which is a multi-channel algorithm that uses empirical relationships to correct for water vapor absorption:

$$T_{ice} = a + bT_4 + cT_5 + d\left[(T_4 - T_5)\sec\theta\right] \quad [3]$$

where T_4 and T_5 are the satellite-measured brightness temperature (K) in the AVHRR thermal channels and θ is the sensor scan angle. The coefficients are determined through a least squares regression, where surface temperatures are regressed against modeled brightness temperatures.

To model radiances in the AVHRR thermal channels, daily temperature and humidity profiles collected by rawinsonde from a Soviet drifting ice station (NP-26) in 1986–87, located near the North Pole, are used to describe atmospheric conditions in each season for input to the LOWTRAN-7 radiative transfer model (Kneizys *et al.*, 1988). Radiances are modeled for sensor scan angles from 0° to 60° in 10° increments. The appropriate sensor response function is applied to the calculated radiances, and radiances are then converted to brightness temperatures. Atmospheric chemical composition, background tropospheric and stratospheric aerosols for the subarctic winter and summer models are used, since no such information is available from the drifting station. The optical properties of Arctic haze have not been extensively measured; model calculations (Blanchet and List, 1983) show that the volume extinction coefficient of Arctic haze is generally of the same order of magnitude as that of tropospheric aerosols. Therefore, the use of tropospheric background aerosols is appropriate.

Directional surface emissivities for snow are modeled as in Dozier and Warren (1982). The single scattering albedo and asymmetry factor in the scattering phase function are calculated from the Mie equations and the directional, wavelength-dependent emissivities are derived from the delta-Eddington approximation to the equation of radiative transfer. The directional emissivities are then integrated with the response function of each AVHRR thermal channel. An energy balance model (Maykut, 1982) is used to determine a range of surface temperatures for each profile, based on the screen-level temperatures and wind speeds at the drifting station for each month.

Overall, the theoretical accuracy (i.e., regression error) of the estimated surface temperatures is approximately 0.1 K. This value will be slightly higher in practice, since the sensor noise has not been taken into account. On average, errors ranging from 0.1 to 1.0 K, depending on season, can be expected when applying coefficients derived for one satellite to data from another, the smallest errors occurring between NOAA-7 and NOAA-9 coefficients and data.

For the retrieval of IST from AVHRR, Local Area Coverage (1.1 km field of view at nadir) data from the NOAA-11 and NOAA-12 satellites collected by Atmosphere Environment Service are used. First-order calibration was performed following the methods described in NOAA (1991a). Additional corrections were applied to the data to account for the nonlinear response of the thermal channels (Weinreb *et al.*, 1990; NOAA, 1991b). The AVHRR scan angle ranges from 0° to approximately 55°.

Since the IST retrieval can only be done for clear sky conditions, and because automated cloud detection in the polar regions is difficult at best (cf., Key and Barry, 1989) images that are clear over the first-year ice site are selected through a visual analysis of various combinations of the AVHRR visible, near-infrared, and thermal channels. However, it appears that even this manual interpretation of the imagery may not be adequate for detecting low-level ice crystal precipitation ("diamond dust") and very thin stratus.

RESULTS

The near-surface air temperature, T_{air}, the surface temperature from the thermocouple buried just beneath the snow surface, T_{snow}, and the temperature based on upwelling longwave radiation, T_{pyrg}, are shown in Figure 1 for May and June, at a solar time of approximately 1000. Values for T_{snow} represent all measurements where the thermocouple was less than 3 cm below the snow-air interface. The snow temperature is typically higher than the other two temperature measurements in the early part of the experiment due to the insulating effect of the overlying snow. Snow temperatures are sometimes greater than the melting point of the snow after the initial stages of melt onset in late June due to warming of the sensor by increased transmission of solar radiation throughout the snow layer (Barber *et al.*, in press). Table 1 provides a statistical comparison of the different measures of "surface" temperature. The two periods in May reflect early spring (8–18 May) and the transition to late spring conditions (20–24 May), when surface air temperatures become warmer

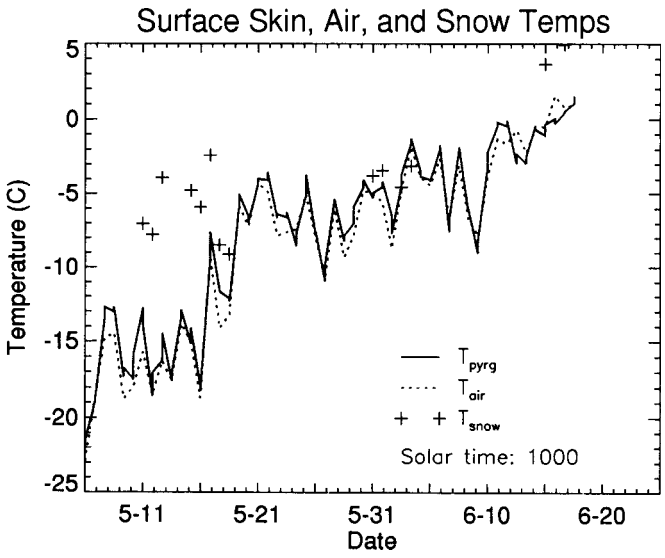

FIG. 1. Near-surface air temperature, temperature measured by a thermocouple just below the surface, and temperature derived from upwelling longwave radiation at the FYI site.

Table 1. Comparison of mean temperatures (˚C) and range of differences for 8–25 May at the FYI site.

	Time Period		
	8–18 May	20–25 May	8–25 May
Mean Temperatures			
T_{pyrg}	-13.39	-6.74	-11.76
T_{air}	-14.74	-7.72	-13.02
$T_{IRtherm}$	-13.90	-6.52	-12.09
T_{s-i}	-8.92	-6.40	-8.15
Temperature Differences			
$T_{IRtherm}$ - T_{pyrg}:			
Mean Difference	-0.51	0.22	-0.33
Standard Deviation	0.62	0.62	0.69
$T_{IRtherm}$ - T_{air}:			
Mean Difference	0.84	1.20	0.93
Standard Deviation	1.32	0.44	1.17
T_{pyrg} - T_{air}:			
Mean Difference	1.35	0.98	1.26
Standard Deviation	1.19	0.90	1.13
$T_{IRtherm}$ - T_{s-i}:			
Mean Difference	-5.69	-0.42	-4.08
Standard Deviation	2.26	2.33	3.36

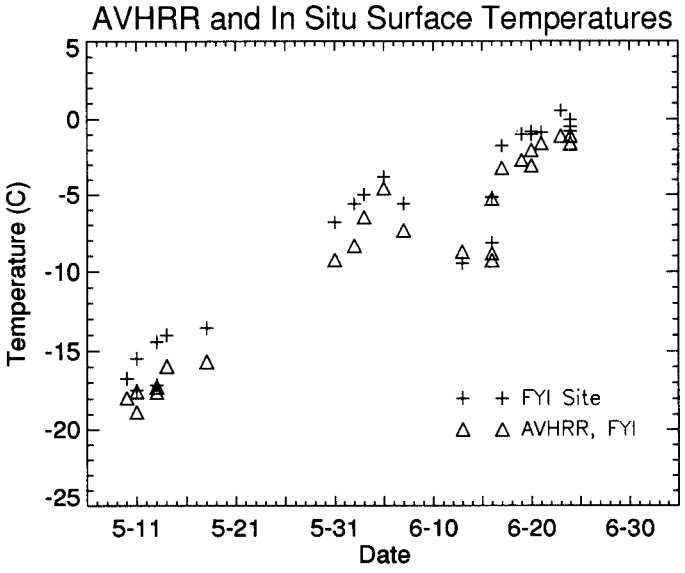

FIG. 2. Surface temperatures estimated from upwelling longwave radiation measured at the surface and from the AVHRR thermal channels at the first-year ice site during May and June.

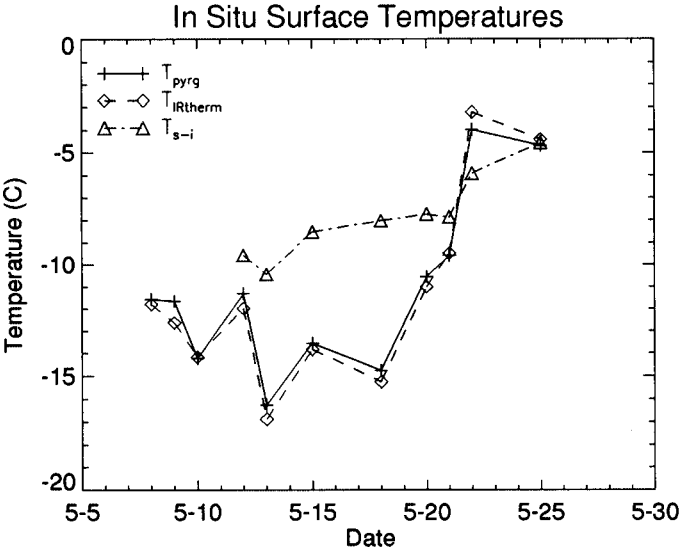

FIG. 3. Surface temperatures measured with the IR thermometer (spatial means) and those based on upwelling longwave radiation. Also shown are measured snow-ice interface temperatures (means).

than T_{s-i}, signifying a change in the direction of heat transport toward warming of the ice surface at the snow/ice interface. $T_{IRtherm}$ and T_{s-i} were grouped and averaged over half hour intervals to coincide with the half hour averages of T_{pyrg} and T_{air}.

Values of T_{AVHRR} are plotted with T_{pyrg} in Figure 2 for May and June. The temperature reported as T_{AVHRR} is a mean of 10 pixels around the FYI site where fields of view contained first-year ice only (i.e., no land), covering approximately 13 km^2, depending on the sensor scan angle. Gaps in the time series result from periods of extensive cloud cover. The maximum time difference between the *in situ* and satellite observations is approximately 20 minutes. Differences between the temperature pairs range from less than 0.1 K to more than 3 K, with the satellite estimates almost always less than the *in situ* values. The differences between T_{AVHRR} and T_{air} (not shown) are less, but the sign of the difference is usually the same. The results are contrary to those presented by Lindsay and Rothrock (in press) where AVHRR-derived ISTs over the Arctic Basin derived using the Key and Haefliger procedure were found to be higher than climatological near-surface air temperatures measured by drifting buoys during April (no May data available) and approximately the same during June.

Temperatures obtained from the IR thermometer, $T_{IRtherm}$, are compared to T_{pyrg} and the snow-ice interface temperature, T_{s-i}, in Figure 3. The systematic difference between $T_{IRtherm}$, and T_{pyrg} over the 8–25 May period is small (0.33˚C difference); $T_{IRtherm}$ measuring slightly lower in early spring (-0.51˚C) and slightly higher during the late spring conditions (0.22˚C). The discrepancy is less than that shown in Figure 2 between the T_{pyrg} and T_{AVHRR} which is not entirely unexpected since T_{AVHRR} represents a sample in time and T_{pyrg} a time average. The difference between $T_{IRtherm}$ and T_{pyrg} at any one time may also be large, as shown by the fairly large standard deviations (Table 1). Absolute differences ranged between 0.02˚C and 1.80˚C. T_{s-i} follows the general increase in heat input to the surface energy budget, with less day-to-day variability because of the insulating effect of the overlying snow cover (Fig. 3). Snow depth averaged 26±9 cm from 8 to 25 May.

DISCUSSION

Andreas (1986) has also observed large discrepancies among surface temperatures measured by different approaches (near-surface thermistors and thermocouple sensors, hand-held pyrometer and near-surface dew point temperature). Much of the

variation in his study was attributed to contamination by solar radiation and suspected sensor instability. In contrast, the temperature differences observed in our study are more likely due to undetected clouds in the imagery, the spatial and temporal variability of the temperature field, incorrect assumptions concerning the surface emissivity and atmospheric conditions, inaccuracies in the model used in the development of the satellite retrieval algorithm, and instrument error.

Undetected Clouds

Despite the multi-spectral approach to the manual selection of clear images, there are conditions where condensed water simply cannot be detected with the spectral information that the AVHRR provides (Key and Barry, 1989). This is particularly true for very thin clouds such as Arctic stratus. Even more difficult to detect are low-level water or ice fogs, the most common being ice crystal precipitation in winter and early spring. The problem in their detection is that they usually exist within the low-level temperature inversion (Kahl *et al.*, 1992) and may result in top-of-atmosphere radiances very close to what would be observed in their absence; i.e., their radiative properties, both shortwave and longwave, are similar to those of the surface. This often equates to a top-of-atmosphere temperature difference of a few degrees or less.

A re-examination of the satellite data after the initial manual cloud cover assessment and a comparison with cloud observations taken at the meteorological station at Resolute Airport indicate that some form of thin cloud may actually have been present over the FYI site at the times of the AVHRR acquisitions. However, as cloud conditions may differ over only a few kilometers, it is impossible to state conclusively how often this problem influences our analysis. While cloud type and opacity were estimated for the entire sky hemisphere during the IR thermometer measurements, additional information is needed concerning clouds that lie along the path between the satellite and the surface temperature measurements.

Spatial and Diurnal Variability of Surface Temperature

Variability of $T_{IRtherm}$ within the 1 km site arises primarily from differences in snow depth, the shadowing effects of sastrugi-like features, and changes in temperature during the time required to cover the transects. Figure 4 illustrates the diurnal variability of skin temperature during May. Shown are all observations of $T_{IRtherm}$ throughout the period, plotted by local time. The apparent relationship between solar zenith angle and skin temperature is biased somewhat by sampling date for times between 1600 hrs and 2000 hrs since these observations were all collected on a single day. However, observations during other times spanned several days during 8 to 24 May, so that the temperature on any specific day does not dominate the plot. From Figure 4 it can be seen that, in order to arrive at a "true" skin temperature for a large area based on field measurements, the variability introduced by the diurnal temperature change can be minimized by sampling during early afternoon. For example, the standard deviation in temperature for measurement sets carried out between approximately 1100 and 1500 hrs. is 0.62˚C, compared to 0.82˚C for all measurement sets. The greatest source of spatial variability is likely due to shadowing. Measurements taken with the shaded versus sunlit aspects of sastrugi (typical height of 10 to 15 cm) filling the entire field of view of the IR thermometer yielded temperature differences of as much as 10˚C in clear sky conditions, but only 1˚C when overcast. In the normal sampling, the IR thermometer was held further away from the surface to yield a larger field of view that typically encompassed a mixture of shadow and sunlit areas, but not necessarily in equal proportions.

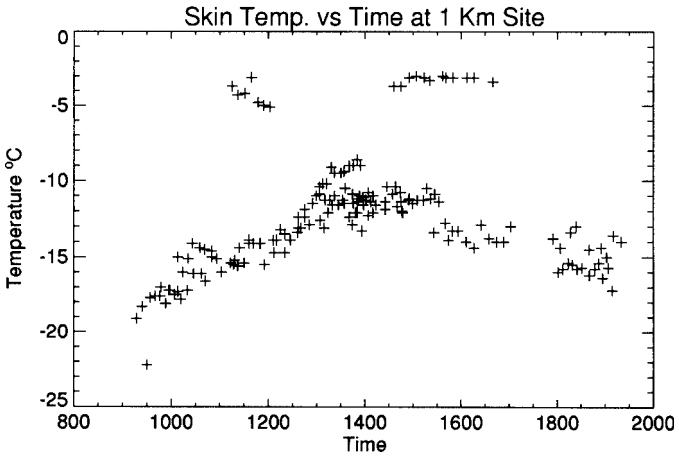

FIG. 4. Temperature measured with the IR thermometer throughout May, plotted as a function of local time.

Figures 5 and 6 show the spatial variability of T_{AVHRR}, $T_{IRtherm}$, and $T_{s\text{-}i}$ throughout May (satellite and *in situ*) and June (satellite only). With the satellite data the variability shown in Figure 5 represents temperatures over a 10 pixel area around the FYI site. There were no open water or thin ice (significantly less than 1 m) areas in the scene. The standard deviation in the temperatures measured with the IR thermometer is up to twice that of the AVHRR-derived ISTs. As noted earlier, minimizing the time to sample the transects would reduce the variability of $T_{IRtherm}$.

The surface temperature may change rapidly in response to radiative forcing. T_{pyrg} represents an average of this temperature over a half hour period. While $T_{IRtherm}$ also represents an average, its value may be biased by the non-systematic number of samples within the averaging period (ranging from 1 to 6), the irregular time increments between samples, and by spatial variability.

Assumptions Made in the Retrieval Procedures

A number of questions arise concerning the assumed properties of the surface and atmosphere affecting the AVHRR data and, potentially, the pyrgeometer measurements. One such assumption concerns the emissivity of the surface for the IR thermometer measurements. All reported observations of $T_{IRtherm}$ are based on an emissivity setting of 0.990, which is the highest setting possible on the instrument. This value is probably appropriate for the broadband emissivity of snow with grain sizes in the 100 – 200 μm range (Dozier and Warren, 1982), but not for the 8 – 14

μm spectral range of the IR thermometer. In that range, the emissivity of snow is closer to 0.993 (Dozier and Warren, 1982). The relationship between thermodynamic temperature T (K), emissivity ε, and radiance L (milliwatts/m^{2}steradian-cm^{-1}) is derived from the Planck function as:

$$T = \frac{c_2\lambda}{1n\left(\frac{\varepsilon c_1\lambda^3}{L} + 1\right)} \quad [4]$$

where c_1 and c_2 are constants ($c_1 = 1.1910659 \times 10^{-5}$ milliwatts/m^2-steradian-cm^{-4} and $c_2 = 1.438833$ cm-K) and λ is the wave number (cm^{-1}). While the difference between the assumed and probable snow emissivity is not large, it does result in a temperature overestimate of approximately 0.3°C.

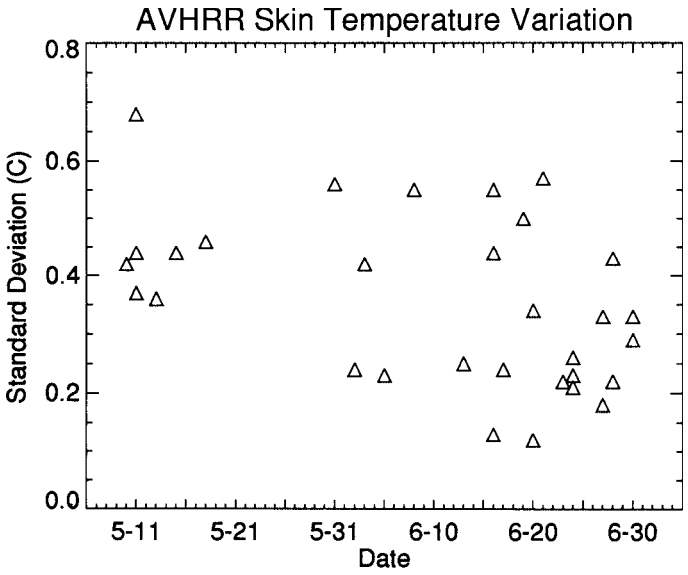

FIG. 5. Variability of satellite-derived surface temperature within a 10-pixel area around the FYI site.

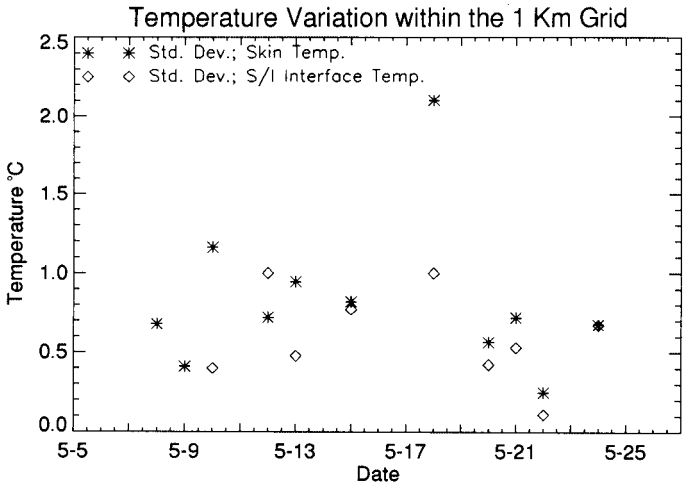

FIG. 6. Variability of surface temperature measured with the IR thermometer and the snow-ice interface temperature around the FYI site.

Additionally, the upwelling radiance measured by the instrument is the sum of the radiation emitted by the surface and the downwelling atmospheric radiation reflected by the surface. (We consider any depletion or addition of radiation from the atmosphere itself to be insignificant given the short atmospheric path from the sensor to the surface.) While the amount of downwelling atmospheric radiation reflected by the surface is relatively small given the high surface emissivity, it does increase the radiance received by the sensor. If corrections for this effect were made, values of $T_{IRtherm}$ would be even lower and closer to the satellite-derived temperatures by an estimated 0.1 K to 0.2 K.

Assumptions concerning atmospheric conditions could play a role in explaining the differences between the satellite-derived and *in situ* temperatures. As described earlier, the retrieval algorithm is based on ice station data from the central Arctic Ocean. The coefficients in [1] were derived for three seasons and in some sense represent the mean conditions during those periods. How do these mean conditions compare with those observed during SIMMS'92? May falls into the transition season of Key and Haefliger (1992), while June falls into their summer season. Differences between the ice station and the SIMMS location (represented by nearby Resolute) are shown in Table 2 for total precipitable water, near-surface air temperature and aerosol optical depths. No information is available on the actual aerosol optical depth at the drifting ice station so that the value shown in the table is the assumed amount used in model calculations. While the surface air temperatures at the two locations (and times) are different, the range of temperatures used in the development of the IST retrieval algorithm is similar to that experienced during SIMMS'92. The water vapor amounts are also similar. Aerosol amounts are different, primarily as a result of stratospheric aerosols from the eruption of Mt. Pinatubo, as observed during AGASP IV (Arctic Gas and Aerosol Sampling Program) over the Beaufort Sea in 1992 (Stone *et al.*, 1993). Although the overall effect of aerosols on the attenuation of upwelling longwave radiation is small, an aerosol amount greater than that expected would produce a lower top-of-atmosphere radiance, which, especially at significantly off-nadir views, would result in an underestimate of IST.

Lastly, there may be a bias in the retrieved ISTs due to AVHRR calibration errors. This may not be trivial; for example, the nonlinear calibration alone can make a difference of more

TABLE 2. Mean precipitable water, surface temperatures, and aerosol optical depths at a drifting ice station and Resolute, N.W.T.

	Ice Station		Resolute	
	Transition[1]	Summer[2]	May	June
Precipitable Water (mm)	4.6	6.6	4.2	7.1
Surface Temperature (°C)	-19.4	-0.9	-13.8	-2.7
Aerosol Optical Depth	0.07[3]	0.07	0.25	0.20

[1] April, May, September, 1987
[2] June - August, 1987
[3] Assumed value for model calculations

than 1˚C. Overall, however, we expect calibration errors to be much less, on the order of 0.1 K to 0.2 K.

Possible Errors in the Calculation of T_{pyrg}

Given that the adjustments to $T_{IRtherm}$ and T_{AVHRR} just discussed will decrease the differences between the two measurements, and given that both of these temperatures are typically lower than that derived from the average upwelling longwave broadband radiation T_{pyrg}, we are left wondering if there are any reasons why T_{pyrg} would be biased.

The vertical placement of the pyrgeometer at 8.9 m above the surface could play a role. Early in the season when temperature inversions are common, the atmosphere between the surface and the sensor is warmer than the surface. Given that the atmosphere is relatively warm, that the surface emissivity is less than unity, and that relative humidities near the surface are high, one would expect an increase in longwave radiation received at the sensor over that emitted by the surface. Radiative transfer calculations of upwelling longwave flux confirm this, although the increase in the estimated physical temperature of the surface is small, 0.3˚– 0.4˚C for a surface temperature of -13˚C. Additionally, the large field of view associated with the pyrgeometer samples the emitted infrared radiation from a much larger area than the hand-held pyrometer, and the IR emitted by the support tower infrastructure and other "non-snow" objects are also sampled. Further experimentation is required to determine the relative effect of these last two points.

Our derivation of L using the pyrgeometer assumes that any solar heating of the instrument dome and subsequent re-radiation to the thermopile is negligible, and that the thermopile temperature is closely approximated by the case temperature as indicated by equation [A6] in the Appendix. There is little reason to believe a large discrepancy in temperature between the thermopile and case thermistor given their close proximity. The net effect of the solar heating of the dome is to increase the calculated value of L (Albrecht and Cox, 1977). Solar heating of the dome is not expected for the inverted pyrgeometer ($L\uparrow$), and, in fact, the case and dome temperature differed on average by only 0.10˚C between 8 and 25 May, with the dome being actually cooler than the case. The opposite was observed for the sky-facing pyrgeometer. Slight heating of the dome for $L\downarrow$ was observed; however, the average, 0.34˚C, is approximately one-tenth the magnitude as that observed by Berdahl and Fromberg (1982). A 0.3˚C change in T_{pyrg} will require a deviation in $L\downarrow$ on the order of 138 Wm^{-2} as estimated using equations [A1] to [A5]. Hence, the small amount of observed solar heating of the $L\downarrow$ dome is not considered to be a factor influencing T_{pyrg}.

CONCLUSIONS

In an effort to validate the satellite retrievals of ice surface temperature, differences between AVHRR-derived ice surface temperature, T_{AVHRR}, and the radiating temperature derived from measurements of upwelling longwave (broadband) radiation, T_{pyrg}, during May and June in the Canadian Arctic were observed to range from less than 0.1˚C to more than 3˚C, with T_{AVHRR} always less than T_{pyrg}. Similarly, the mean temperatures of spatially-distributed measurements made by a hand-held IR thermometer, $T_{IRtherm}$, were typically less than T_{pyrg}, although the differences were not as great as between T_{AVHRR} and T_{pyrg}. The temperature measured by a thermocouple placed approximately 1 cm below the snow-air interface illustrates the insulating quality of the overlying snow, being higher than the radiating temperature in the early part of the season.

While these results can be explained to a limited extent by instrument calibration, incorrect assumptions of the surface emissivity and atmospheric conditions, and model inaccuracies, the main issue with a validation exercise such as this is in the definition of the "correct" surface temperature and of the method chosen to measure this temperature. The temperature of interest is the radiating temperature, not the near-surface snow temperature or the near-surface air temperature. In theory, the upwelling longwave radiation can be used to determine this temperature, but in practice care must be taken to obtain an accurate value. The spatially-averaged temperatures measured with the IR thermometer suggest a possible negative bias in the AVHRR-derived temperatures, with a possible simple correction for this bias. However, the spatial and temporal variations in skin temperatures observed during the sampling of the 1 km transects with the IR thermometer are too great to permit a determination of a bias with any certainty. We conclude that there is probably a negative bias in T_{AVHRR} as computed here, on the order of 0.5˚C to 1˚C. To determine the actual magnitude and source of this bias we need a well-calibrated, airborne radiometer measuring in the same spectral bands as the AVHRR (to reduce the atmospheric effects and to obtain adequate spatial coverage), combined with refined surface observations that include faster sampling, more precise instrumentation, and more detailed observations on cloud properties and distributions relative to the AVHRR scan.

ACKNOWLEDGEMENTS

This work was supported by NSF grants DPP-9113958 and DPP-9024114, NASA grant NAGW-3437, and ONR grant N00014-90-J-1840. Canadian funding was provided by the Province of Ontario (Centre of Excellence grant) and the Natural Sciences and Engineering Research Council (NSERC). Thanks are due to the principal investigators of the SIMMS project, E. LeDrew and D. Barber. We also thank other members of the SIMMS group for help in the field, and M. Shokr for processing the AVHRR data.

APPENDIX: ESTIMATION OF ERROR ASSOCIATED WITH T_{pyrg}

Assuming that all errors are random and independent, the uncertainty associated with the estimation of T_{pyrg} may be approximated following Bevington (1969) as:

$$\Delta T_{pyrg} = 0.25 T_{pyrg}\left(\frac{\Delta X}{X}\right) \qquad [A1]$$

where $X = L\uparrow_{surf}/\sigma\varepsilon$, σ is the Stefan-Boltzman constant, and ε is the surface emissivity. The uncertainty in X is:

$$\frac{\Delta X}{X} = \left[\frac{\Delta L\uparrow^2_{surf}}{L\uparrow^2} + \frac{\Delta\varepsilon^2}{\varepsilon^2} - \frac{2\,\mathrm{cov}(L\uparrow_{surf}, \varepsilon)^2}{(L\uparrow_{surf}\ \varepsilon)^2} \right]^{\frac{1}{2}}, \quad [A2]$$

but may be reduced to:

$$\frac{\Delta X}{X} = \left[\frac{\Delta L\uparrow^2_{surf}}{L\uparrow^2} \right]^{\frac{1}{2}} \quad [A3]$$

since both the covariance term and the error associated with the emissivity in [A2] will be much smaller than that associated with $L\uparrow_{surf}$. Rearranging [2] from the Methods section gives:

$$L\uparrow_{surf} = L\uparrow - (1-\varepsilon)L\downarrow, \quad [A4]$$

from which ΔL may be estimated with:

$$\Delta L\uparrow_{surf} = (\Delta L\uparrow^2 + (1-\varepsilon)^2\,\Delta L\downarrow^2)^{\frac{1}{2}}, \quad [A5]$$

assuming any error in the selected ε to be small. The measured infrared flux is estimated using:

$$L(\uparrow or \downarrow) = F + \sigma T^4_{case} \quad [A6]$$

where F is the infrared flux as derived using the measured thermopile voltage output and appropriate calibration, and T_{case} is the internal instrument temperature (K) which is supplied by the case thermistor. The uncertainty of each flux measurement is:

$$\Delta L(\uparrow or \downarrow) = \left[\Delta F^2 + \left(\frac{4\sigma T^4_{case}\Delta T_{case}}{T_{case}} \right)^2 \right]^{\frac{1}{2}} \quad [A7]$$

For example, if from [A7] ΔT_{case} is 0.2 K and ΔF is 1% of the average thermopile measured flux (e.g., F = 14.9 Wm^{-2} for $L\uparrow$ and 45.59 Wm^{-2} for $L\downarrow$), and T_{case} is 258.15 K, then estimates of ΔL are 0.794 Wm^{-2} for $L\uparrow$ and 0.903 Wm^{-2} for $L\downarrow$. Using [A5], [A3], and [A1], ΔT_{pyrg} is 0.205 K and $\Delta L\uparrow_{surf}$ = 0.794 Wm^{-2} for $L\uparrow$ = 24 9.08 Wm^{-2} and T_{pyrg} = 258.10 K, as is the case for solar noon on 13 May 1992.

REFERENCES

ALBRECHT, B., and COX, S.K. 1977. Procedures for improving pyrgeo- meter performance. Journal of Applied Meteorology 16: 188–197.

ANDREAS, E. L. 1986. A new method of measuring the snow surface temperature. Cold Regions Science and Technology 12: 139–156.

BARBER, D.G., REDDAN, S.P., and LeDREW, E.F. In press. Statistical characterization of the geophysical and electrical properties of snow on landfast first-year ice. Journal of Geophysical Research (Oceans).

BARTON, I.J. 1992. Satellite-derived sea surface temperatures – a comparison between operational, theoretical, and experimental algorithms. Journal of Applied Meteorology 31:433–442.

BERDAHL, P., and FROMBERG, R. 1982. The thermal radiance of clear skies. Solar Energy 29:299–314.

BEVINGTON, P.R. 1969. Data reduction and error analysis for the physical sciences. Toronto: McGraw-Hill, Inc. 336 p.

BLANCHET, J., and LIST, R. 1983. Estimation of optical properties of arctic haze using a numerical model. Atmosphere-Ocean 21:444–465.

DOZIER, J., and WARREN, S.G.1982. Effect of viewing angle on the infrared brightness temperature of snow. Water Resources Research 18(5):1424–1434.

KAHL, J.D., SERREZE, M.C., and SCHNELL, R.C. 1992. Tropospheric low-level temperature inversions in the Canadian Arctic. Atmosphere-Ocean 30(4):511–529.

KEY, J., and BARRY, R.G. 1989. Cloud cover analysis with arctic AVHRR data: 1. cloud detection. Journal of Geophysical Research 94(D15):18521–18535.

KEY, J., and HAEFLIGER, M. 1992. Arctic ice surface temperature retrieval from AVHRR thermal channels. Journal of Geophysical Research 97(D5):5885–5893.

KNEIZYS, F.X., SHETTLE, E.P., ABREU, L.W., CHETWYND, J.H., ANDERSON, G.P., GALLERY, W.O., SELBY,J.E.A., and CLOUGH, S.A. 1988. Users Guide to LOWTRAN 7. AFGL-TR-88-0177, Environmental Research Papers No. 1010. U.S. Air Force Geophysics Laboratory, Hanscom AFB, MA. 137 p.

LINDSAY, R.W., and ROTHROCK, D.A. In press. Arctic sea ice surface temperature from AVHRR. Journal of Climate.

MAYKUT, G.A. 1982. Large-scale heat exchange and ice production in the central Arctic. Journal of Geophysical Research 87(C10): 7971–7984.

NOAA. 1991a. NOAA Polar Orbiter Data User's Guide. U.S. Dept. of Commerce. National Oceanic and Atmospheric Administration, NESDIS, February.

NOAA. 1991b. Amendments to NOAA Technical Memorandum 107, Appendix B. U.S. Department of Commerce. National Oceanic and Atmospheric Administration, NESDIS, May 14.

RYZNAR, E., and WEBER, M.R. 1982. Comments on the performance of pyrgeometers with silicon domes. Journal of Applied Meteorology 14:1297–1302.

STONE, R.S., KEY, J., and DUTTON, E. 1993. Properties and decay of stratospheric aerosols in the Arctic following the 1991eruptions of Mount Pinatubo. Geophysical Research Letters 20(21): 2359–2362.

WEINREB, M.P., HAMILTON, G., and BROWN, S. 1990. Nonlinearity corrections in calibration of advanced very high resolution radiometer infrared channels. Journal of Geophysical Research 95(C5):7381–7388.

WEISS, A. 1981. On the performance of pyrgeometers with silicon domes. Journal of Applied Meteorology 20:962–965.

———. 1982. Reply to Ryzanar and Weber. Journal of Applied Meteorology 21:1211–1212.

WICK, G.A., EMERY, W.J., and SCHLUESSEL, P. 1992. A comprehensive comparison between satellite-measured skin and multichannel sea surface temperature. Journal of Geophysical Research 97(C4):5569–5595.